

## ELECTROCHEMICAL PERFORMANCE OF Sn DOPED Mn<sub>3</sub>O<sub>4</sub> / GRAPHENE FOR SUPERCAPACITORS

L. M. DONG<sup>a,b,\*</sup>, L. CHEN<sup>a</sup>, M. C. CAO<sup>a</sup>, S. WANG<sup>a</sup>, H. Y. FU<sup>a</sup>

<sup>a</sup>*College of Materials Science and Engineering, Harbin University of Science and Technology, Harbin, China*

<sup>b</sup>*Key Laboratory of Engineering Dielectrics and Its Application, Ministry of Education, Harbin University of Science and Technology, Harbin, China*

Mn<sub>3</sub>O<sub>4</sub> was prepared by hydrothermal method with 180 °C as reaction temperature and 10 h as reaction time. The obtained samples were bar-like samples with high purity were evaluated by X-ray diffraction (XRD) and scanning electron microscopy (SEM). The electrochemical performance of Mn<sub>3</sub>O<sub>4</sub> was improved by Sn-doping. The specific capacitance of the composites obtained by compounding the modified materials with graphene was greatly increased and their cyclic voltammetric curves were rectangular, which shows that the graphene modified Mn<sub>3</sub>O<sub>4</sub> has a pleasurable development prospect. For the pure Mn<sub>3</sub>O<sub>4</sub>, Sn-Mn<sub>3</sub>O<sub>4</sub> and Sn-Mn<sub>3</sub>O<sub>4</sub> / graphene composite, the specific capacitance of 21 F·g<sup>-1</sup>, 30 F·g<sup>-1</sup> and 215 F·g<sup>-1</sup> were manifested by electrochemical work station, respectively. The results show that stannum and graphene greatly enhances the electrochemical performance of Mn<sub>3</sub>O<sub>4</sub>.

(Received November 30, 2018; Accepted January 4, 2019)

*Keywords:* Supercapacitor, Mn<sub>3</sub>O<sub>4</sub>, Sn, Graphene, Hydrothermal synthesis

### 1. Introduction

The embarrassment of energy using has led us to continue to develop new technologies for energy conversion [1] and energy storage [2]. At present, fuel cells, lithium ion batteries, dye-sensitized solar cells and supercapacitors are the most widely used in energy storage [3-6]. As a new energy storage component, supercapacitors not only have high power density, long cycle life, but also are environmentally friendly, green and non-polluting, and have broad application prospects [7-11]. The performance of the electrode material is a key factor affecting the performance of the capacitor [12]. Therefore, the preparation of a high-performance electrode material with high capacitance and good cycle stability is the research focus of the supercapacitor [13]. In recent years, manganese oxide compounds have been widely used in supercapacitor electrode materials because of their ideal theoretical capacitance, low cost, and excellent performance [14, 15]. Mn<sub>3</sub>O<sub>4</sub> has become one of the potential electrode materials for supercapacitors due to its microstructural controllability [16]. However, due to the poor conductivity of manganese oxide, its further development in this respect is limited. At present, doping other metal atoms or combining Mn<sub>3</sub>O<sub>4</sub> with a carbon material with good conductivity is an important means to improve the electrochemical performance of Mn<sub>3</sub>O<sub>4</sub> [17].

Zhao yufeng et al. [18] used Pluronic P123 (EO<sub>20</sub>PO<sub>70</sub>EO<sub>20</sub>) as both structure-directing agent and carbon source to synthesize Sn-doped Mn<sub>3</sub>O<sub>4</sub>/C nanocomposite. A high specific capacitance of 216 F·g<sup>-1</sup> was achieved and 93% capacitance retention remained after 10,000 charge/discharge cycles. With potassium permanganate as precursor and hydrazine hydrate as reductant, Song YZ et al. [19] prepared Mn<sub>3</sub>O<sub>4</sub> / Double-Walled Carbon Nanotubes Nanocomposites for supercapacitors by chemical precipitation method. The high power density, large specific surface area, good catalytic performance, good conductivity and stability of Mn<sub>3</sub>O<sub>4</sub> nanoparticles were fully utilized. Anilkumar KM et al. [20] prepared a nanocomposite of Mn<sub>3</sub>O<sub>4</sub> and reduced graphene oxide by simple, physical mixing of the components and its suitability as electrode material for high power supercapacitors was analysed by detailed electrochemical

---

\*Corresponding author: donglimin@hrbust.edu.cn

characterization. In this study,  $\text{Mn}_3\text{O}_4$ ,  $\text{Sn-Mn}_3\text{O}_4$ , and  $\text{Sn-Mn}_3\text{O}_4$  / graphene have been synthesized by hydrothermal method. The performance of  $\text{Sn-Mn}_3\text{O}_4$  / graphene electrodes was compared with pure  $\text{Mn}_3\text{O}_4$  and  $\text{Sn-Mn}_3\text{O}_4$ , and showed attractive high capacitive performance, implying the great potential of this material for high performance energy storage devices.

## 2. Materials and methods

### 2.1. Materials and preparation

By hydrothermal method,  $\text{NH}_3\cdot\text{H}_2\text{O}$ (AR) and  $\text{MnCl}_2$ (AR) were used as raw materials. The mixture of  $\text{NH}_3\cdot\text{H}_2\text{O}$ (AR) and  $\text{MnCl}_2$ (AR) was dissolved evenly and 1%, 2%, 5%, 10% molar ratio of  $\text{SnCl}_4$ (AR) and composite graphene were added separately. After full mixing,  $\text{NH}_3\cdot\text{H}_2\text{O}$ (AR) was added to adjust the pH value until  $\text{pH} = 7$ . Composite  $\text{Mn}_3\text{O}_4$  material was prepared by filling the reactor at appropriate temperature and holding time. In this experiment, the nickel foam was used as the collector. The first step was to cut the nickel foam into 2 cm and 1 cm rectangle. Then removed the surface oxide by dilute hydrochloric acid. The electrode active material was mixed with acetylene black and polytetrafluoroethylene in 8:1:1 ratio, and then adjusted to paste and smeared on the cleaned nickel foam surface, then dried in the vacuum oven until the quality of the electrode piece remained unchanged.

### 2.2. Characterization

The crystal structures of the product was identified by X-ray diffraction (XRD, PANalytical X'Pert PRO MPD, Holland) with  $\text{Cu-K}\alpha$  radiation ( $\lambda=0.154056$  nm), the scanning speed of  $10^\circ/\text{min}$  and scanning range of  $5^\circ - 90^\circ$ . Morphological features of the samples were observed using Field emission scanning electron microscopy (FE-SEM, Sirion200, Philip). Then RST5000 model Electrochemical Workstation was used to determine the electrochemical performance of active electrode.

## 3. Result and discussion

### 3.1. Phase characterization

Fig. 1 showed the XRD patterns of  $\text{Mn}_3\text{O}_4$ . The angle of the  $2\theta$  of the XRD scan is 10 degrees ~80 degrees and the crystal phase of  $\text{Mn}_3\text{O}_4$  is characterized. Compared with the standard PDF card 89-4837, the XRD spectra showed that the XRD spectra were basically identical and there was no heterocyclic peak in other crystalline phases.

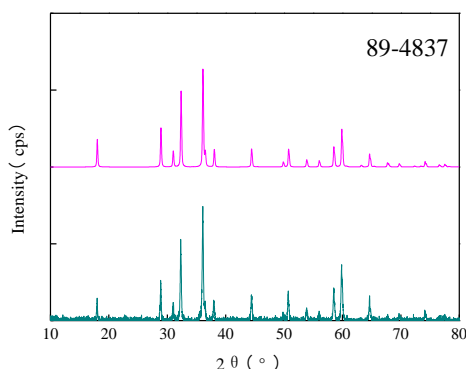


Fig. 1. XRD patterns of  $\text{Mn}_3\text{O}_4$  at  $180^\circ\text{C}$  for 10 h.

Fig. 2 is a scanning electron microscope (SEM) photograph of  $\text{Mn}_3\text{O}_4$  at  $180^\circ\text{C}$  for 10 h. As can be seen from Fig. 2, the powder particles are uniform and fine rod-like particles, and the size is very uniform. It may be that the reaction time was sufficient and the grain had enough time to grow.

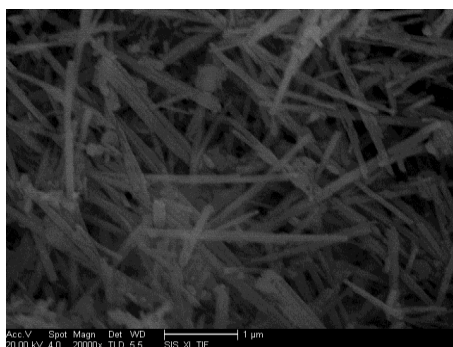


Fig. 2. The SEM images of  $Mn_3O_4$  at 180 °C for 10 h

### 3.2. Electrochemical properties of Sn-doped $Mn_3O_4$

Fig. 3 shows the cyclic voltammetric curves of  $Mn_3O_4$  samples with different doping concentration of Sn in the range of -0.1-0.9 V (vs SCE) voltage and scanning rate of 10  $mV \cdot s^{-1}$  and 0.5  $mol \cdot L^{-1}$  electrolyte, respectively. From Figure 3-3, it can be seen that the CVA curves are approximately rectangular, indicating that the capacitance of the material is good and the current can respond quickly when the scan is converted. It can be seen from the diagram that the response currents of different doping concentrations are different. The specific capacitance of a, b, c, d and e can be calculated from the formula  $CF = i \cdot (vwm)^{-1}$  as 21  $F \cdot g^{-1}$ , 27  $F \cdot g^{-1}$ , 30  $F \cdot g^{-1}$ , 29  $F \cdot g^{-1}$  and 26  $F \cdot g^{-1}$ , respectively. It shows that the specific capacitance increases with the increase of n (Sn): n (Mn) doping ratio.

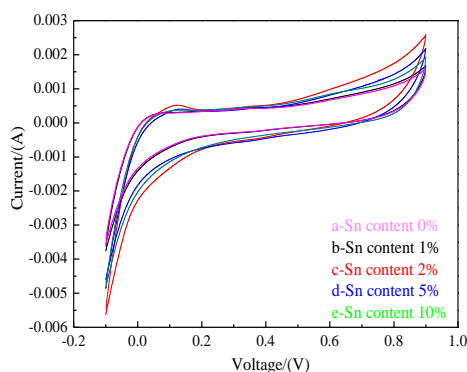


Fig. 3. cyclic voltammetry of  $Mn_3O_4$  with different Sn content.

Fig. 4 shows a cyclic volt of different scan rate with 10  $mV \cdot s^{-1}$ , 20  $mV \cdot s^{-1}$ , 50  $mV \cdot s^{-1}$  and 100  $mV \cdot s^{-1}$  for a Sn- $Mn_3O_4$  sample with a Sn content of 2%. When the scan rate is increased from 10  $mV \cdot s^{-1}$  to 20  $mV \cdot s^{-1}$ , the response current increases and the added multiple is similar to the scan rate. It shows that the electrode material can still maintain good capacitance performance when the scanning rate is not high. However, when the scanning speed continues to increase, the response current does not increase in proportion to the scan rate even when the temperature is increased from 20  $mV \cdot s^{-1}$  to 50  $mV \cdot s^{-1}$  to 100  $mV \cdot s^{-1}$ . The main reason for this phenomenon is that although the acceleration of the scanning speed would increase the speed of the Faraday capacitance reaction to some extent, the response current can be increased when the scanning speed is low, but the ion diffusion speed cannot be increased when the scanning speed is too fast. Keeping up, the speed of the Faraday's capacitance response is limited, so that the magnitude of the response current cannot keep up, so the response current increases to a lesser extent. The sample can still retain the rectangular characteristic at high scanning speed, and its specific capacitance is not attenuated too much, indicating that the electrode material has good reversibility.

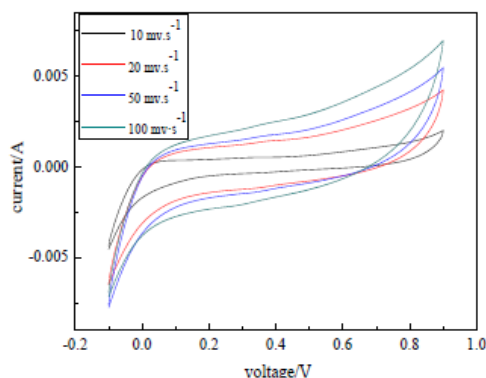


Fig. 4. cyclic voltammety of  $Mn_3O_4$  with 2 % Sn at different scanning speed.

Fig. 5 shows the AC impedance spectra of the Sn- $Mn_3O_4$  electrode at 1%, 2%, 5%, and 10% Sn. As can be seen from the figure, when the doping amount of Sn is small,  $R_s$  is reduced, because a small amount of Sn can also increase the diffusion and transport speed of the overall electrolyte ions in the active material. The resistance of  $Mn_3O_4$  is relatively high, which corresponds to the results of the cyclic voltammogram of each sample in Fig. 3, but when the concentration of Sn element is too large, the clogging of trimanganese tetraoxide is also caused to hinder the ion transfer, so that the electrode electrochemical performance is degraded. In addition, regardless of the proportion of the Sn element added, the slope of the impedance spectrum in the low frequency region is significantly greater than  $45^\circ$ , indicating that each sample has good capacitance characteristics.

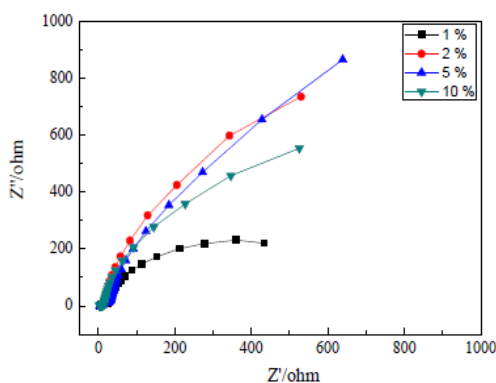


Fig. 5. AC impedance spectroscopy of  $Mn_3O_4$  with different Sn content.

The fact that the Sn element plays a role in improving the electrochemical performance in  $Mn_3O_4$  can be explained by the fact that the addition of Sn ions of different valence states produces a partially deficient Sn ion among the  $Mn_3O_4$ , which improves the conductivity of  $Mn_3O_4$ . This further increases the electrochemical performance of the overall active material. When the content of Sn was insufficient in the material, the conductive particles generated by the electrode material were insufficient, so that the electrode material also had a space for improving its capacitance characteristics. However, when the Sn element was too much, the channel for ion in and out in the crystal structure of the  $Mn_3O_4$  was blocked, forcing the conductivity of the electrode material to decrease and the capacitance characteristics were also deteriorated, so that only in the range of suitable Mn and Sn ratios can obtain an electrode material with good capacitance performance. At the same time, the addition of Sn can prevent the irreversible reaction of  $Mn_3O_4$ , which is beneficial to increase the stability of the electrode material.

### 3.3. Electrochemical properties of Sn-doped $\text{Mn}_3\text{O}_4$ /graphene composites

Fig. 6 is a TEM photograph of the Sn- $\text{Mn}_3\text{O}_4$ /graphene material.

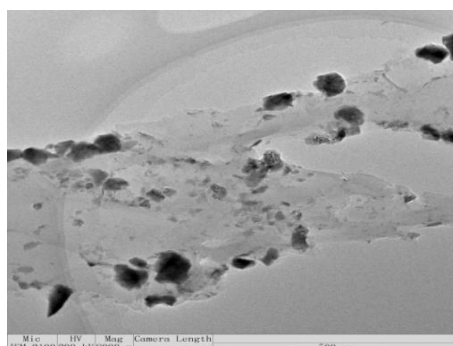


Fig. 6. TEM images of Sn- $\text{Mn}_3\text{O}_4$  graphene composite.

It is found from Fig. 6 that  $\text{Mn}_3\text{O}_4$  has also been successfully grown on the surface of graphene, and the composite material has the same lamellar structure as graphene and the  $\text{Mn}_3\text{O}_4$  particles can also be seen in the figure. The particle size is very small and reaches the nanometer level. From the distribution, the distribution of  $\text{Mn}_3\text{O}_4$  in the composite material is relatively dispersed, which indicates that it plays a better carrier role in the composite graphene and is related to  $\text{Mn}_3\text{O}_4$ . The combination is very tight.

Fig. 7 shows that cyclic voltammetry curve of Sn- $\text{Mn}_3\text{O}_4$ /graphene composite with different graphene concentrations of 0%, 1%, 2%, 5%, and 10% has a scanning speed of  $10 \text{ mV}\cdot\text{s}^{-1}$  in a  $0.5 \text{ mol}\cdot\text{L}^{-1} \text{ Na}_2\text{SO}_4$  electrolyte.

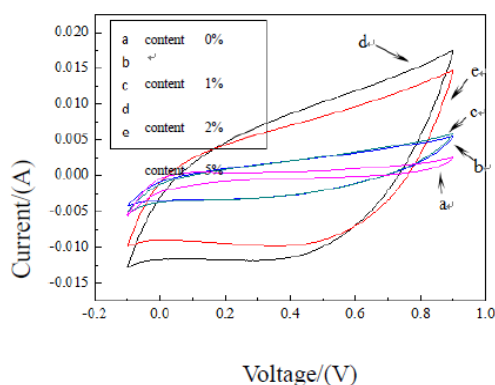


Fig. 7. cyclic voltammetry of Sn-  $\text{Mn}_3\text{O}_4$ / graphene composites with different graphene content.

It can be seen from Fig. 7 that the addition of graphene increases the response current of the electrode material. And as the content of graphene increases, the cyclic voltammetry curve is closer to a rectangular shape and the specific capacitance is greatly improved by calculation. Among them, the specific capacitance is 5% of the graphene concentration of the electrode, the specific capacitance can reach  $215 \text{ F}\cdot\text{g}^{-1}$ .

Fig. 8 shows the cyclic volt-ampere curve of Sn- $\text{Mn}_3\text{O}_4$ /graphene electrode with a graphene content of 5% at a scan rate of  $10 \text{ mV}\cdot\text{s}^{-1}$ ,  $20 \text{ mV}\cdot\text{s}^{-1}$ ,  $50 \text{ mV}\cdot\text{s}^{-1}$ , and  $100 \text{ mV}\cdot\text{s}^{-1}$ , respectively. That can be seen as the cyclic voltammetry scan speed increases, the integral area of the cyclic voltammetry curve decreases significantly. The shape of the curve will become closer to the elliptical shape, indicating that the Sn- $\text{Mn}_3\text{O}_4$ /graphene composite does not have good rate performance. And as the scanning speed increases, the response current of the cyclic voltammetry curve does not increase exponentially. It is indicated that the Sn- $\text{Mn}_3\text{O}_4$ /graphene electrode with a

graphene content of 5% is not suitable for operation under high current conditions.

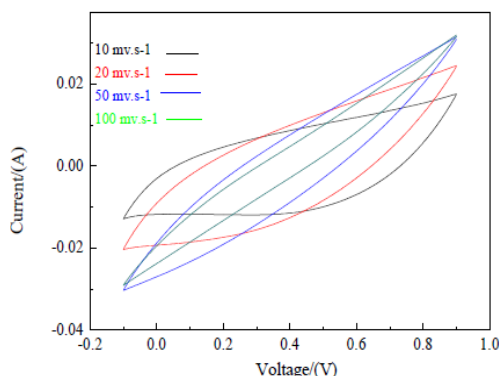


Fig. 8. cyclic voltammetry of Sn- Mn<sub>3</sub>O<sub>4</sub>/ graphene composites with 5 % graphene at different scanning speed.

Fig. 9 shows the AC impedance spectra of Sn-Mn<sub>3</sub>O<sub>4</sub>/graphene electrodes with graphene content of 1%, 2%, 5%, and 10%, respectively. It can be seen from Figure 3-8 that when the composite amount of graphene changes, R<sub>s</sub> decreases slightly with the increase of graphene content. The reason may be that the conductivity of graphene is much better than that of Mn<sub>3</sub>O<sub>4</sub>. Therefore, as the content of graphene in the electrode material increases, R<sub>s</sub> decreases. In the low frequency region of the impedance spectrum, it can be seen that the slope is greater than 45°. It is found that the Sn-Mn<sub>3</sub>O<sub>4</sub>/graphene composite has good capacitance characteristics.

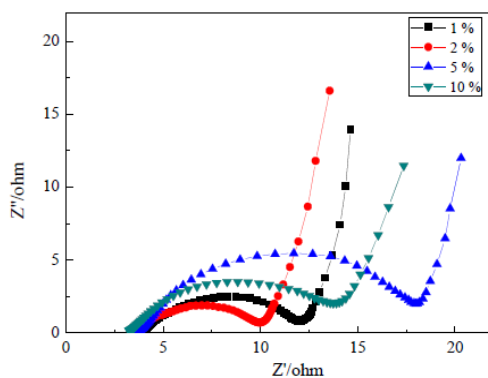


Fig. 9. AC impedance spectroscopy of Sn- Mn<sub>3</sub>O<sub>4</sub>/ graphene composites with different graphene content.

#### 4. Conclusions

Finally, conclusions and future work are summarized. Sn-modified Mn<sub>3</sub>O<sub>4</sub> material was prepared by hydrothermal method and its electrochemical properties were tested. When the content of Sn element reaches 2%, the Sn modified Mn<sub>3</sub>O<sub>4</sub> material has better electrochemical performance and the introduction of Sn element increases the stability of the electrode material. The composite material obtained by compounding this material with 5 wt.% graphene had been analyzed by cyclic voltammetry and AC impedance method. It was found that the capacitance characteristics of the composite material were greatly improved and specific capacitance of 21 F·g<sup>-1</sup>, 30 F·g<sup>-1</sup> and 215 F·g<sup>-1</sup> were displayed for the pure Mn<sub>3</sub>O<sub>4</sub>, Sn-Mn<sub>3</sub>O<sub>4</sub> and Sn-Mn<sub>3</sub>O<sub>4</sub> / graphene composite, respectively. Therefore, graphene can be used to improve Mn<sub>3</sub>O<sub>4</sub> with outstanding development prospects.

## Acknowledgments

This work was financially supported by Natural Science Foundation of Heilongjiang Province (QC06C026).

## References

- [1] G. Dennler, M. C. Scharber, T. Ameri, P. Denk, K. Forberich, C. Waldauf, C. J. Brabec, *Advanced Materials* **20**(3), 579 (2010).
- [2] J. J. Li, J. Claude, L. E. Norena-Franco, S. I. Seok, Q. Wang, *Chemistry of Materials* **20**(20), 6304 (2016)
- [3] L. He, P. Du, Y. Z. Chen, H. W. Lu, X. Cheng, B. Chang, Z. Wang, *Renewable & Sustainable Energy Reviews* **71**, 388 (2017).
- [4] J. W. Fergus, *Journal of Power Sources* **195**(4), 939 (2010).
- [5] X. Wang, L. Zhi, K. Müllen, *Nano Letters* **8**(1), 323 (2008).
- [6] P. Huang, C. Lethien, S. Pinaud, K. Broussek, R. Laloo, V. Turq, M. Respaud, A. Demonrtiere, B. Daffos, P. L. Taberna, B. Chaudret, Y. Gogotsi, P. Simon, *Science* **351**(6274), 691 (2016).
- [7] L. Hao, X. Li, L. Zhi., *Advanced Materials* **25**(28), 3899 (2013).
- [8] Z. S. Wu, K. Parvez, X. L. Feng, K. Müllen, *Nature Communications* **4**(9), 2487 (2013).
- [9] X. Xiao, X. Peng, H. Y. Jin, T.Q. Li, C. C. Zhang, B. Gao, B. Hu, K.F. Huo, J. Zhou, *Advanced Materials* **25**(37):4954 (2013).
- [10] Z. Li, Z. W. Xu, X. H. Tan, H. L. Wang, C. M. B. Holt, T. Stephenson, B. C. Olsen, D. Mitlin, *Energy & Environmental Science* **6**(3), 871 (2013).
- [11] M. Beidaghi, Y. Gogotsi, *Energy & Environmental Science* **7**(3), 867 (2014).
- [12] Y. H. Zhao, M. X. Liu, X. X. Deng, Ling Miao, P. K. Tripathi, X. M. Ma, D. Z. Zhu, Z. J. Xu, Z. X. Hao, L. H. Gan, *Electrochimica Acta* **153**, 448 (2015)
- [13] X. Zhao, H. W. Dong, Y. Xiao, H. Hu, Y. J. Cai, Y.R. Liang, L. Y. Sun, Y. L. Liu, M. T. Zheng, *Electrochimica Acta* **218**, 32 (2016).
- [14] S. He, W. Chen, *Journal of Power Sources* **262**(9), 391 (2014).
- [15] C. Moreno, C. Munuera, S. Valencia, F. Kronast, X. Obradors, C. Ocal, *Nano Letters* **10**(10), 3828 (2010).
- [16] Y. Dan, H. Lin, X. Liu, H. Lu, J. Zhao, Z. Shi, Y. Guo, *Electrochimica Acta* **83**(12), 175 (2012).
- [17] J. Y. Qu, Y. J. Li, C. P. Li, L. Shi, G. H. Shao, F. Gao, *Carbon* **77**(3), 1196 (2014).
- [18] Y. Zhao, W. Ran, D. B. Xiong, L. Zhang, J. Xu, F. Gao, *Materials Letters* **118**(3), 80 (2014).
- [19] Y. Z. Song, R. X. Zhao, K. K. Zhang, J. J. Ding, X. M. Lv, M. Chen, J. M. Xie, *Electrochimica Acta* **230**, 350 (2017).
- [20] K. M. Anilkumar, M. Manoj, B. Jinisha, V. S. Pradeep, S. Jayalekshmi, *Electrochimica Acta* **236**, 424 (2017).